

**The Kormendy relation for early-type galaxies. Dependence on
the magnitude range.**

A. Nigoche-Netro¹, A. Ruelas-Mayorga² and A. Franco-Balderas²

Instituto de Astronomía. Apartado Postal 70-264. Ciudad Universitaria. México, D.F.
México.

Received _____; accepted _____

ABSTRACT

Due to an result from a recently published paper (Nigoche-Netro *et al.* 2007) that states that the intrinsic dispersion of the Kormendy Relation (KR) for Early-Type Galaxies (ETGs) depends on the magnitude range within which the galaxies are contained, we decided to investigate whether the magnitude range has also an influence over the values of the coefficients of the KR; α (zero point) and β (slope). We perform numerical simulations and analysis of these coefficients for 4 samples of galaxies, which contain an approximate total of 9400 ETGs in a relatively ample magnitude range ($\langle \Delta M \rangle \sim 6 - mag$).

We calculate the values of the coefficients of the KR in two ways: i) We consider the faintest galaxies in each sample and we progressively increase the width of the magnitude interval by inclusion of the brighter galaxies (increasing magnitude intervals), and ii) we consider narrow magnitude intervals of the same width ($\Delta M \leq 1.0 - mag$) over the whole magnitude spectrum available (narrow magnitude intervals). The main results we find are as follows: i) In both increasing and narrow magnitude intervals the KR coefficients change systematically as we consider brighter galaxies, ii) non-parametric tests show that there is an underlying trend in the values of the slope of the KR, iii) this trend shows a maximum around absolute magnitude $M_B \sim -18 \pm 1$, and iv) the values of the slope of the KR, in narrower magnitude intervals, keep on having an underlying trend even though their values are closer to 5 (expected value according to the magnitude definition). The analysis of the results makes us conclude that the values of the KR coefficients depend on the width of the magnitude range and the brightness of galaxies within the magnitude range. This dependence is due to the fact that the distribution of galaxies in the $\log(r_e) - \langle \mu \rangle_e$ plane depends on luminosity and that this distribution is not

symmetrical, that is, the geometric shape of the distribution of galaxies in the $\log(r_e) - \langle \mu \rangle_e$ plane plays an important role in the determination of the values of the coefficients of the KR.

Instituto de Astronomía. Apartado Postal 70-264. Ciudad Universitaria. México, D.F.
México.

¹Instituto de Matemáticas y Física Fundamental, C/ Serrano 113 bis, Madrid, España, 28006. e-mail: alberto.n@imaff.cfmac.csic.es

²Instituto de Astronomía. Apartado Postal 70-264. Ciudad Universitaria. México, D.F. México. e-mail: rarm@astroscu.unam.mx, alfred@astroscu.unam.mx

1. Introduction

It is a well known fact that the structural parameters of ordinary ETGs follow the Fundamental Plane (FP) relation (Djorgovsky & Davis 1987; Dressler *et al.* 1987). The FP relation is usually expressed as a correlation among the *logarithm of the effective radius* ($\log(r_e)$), *effective mean surface brightness* ($\langle \mu \rangle_e$) and *logarithm of the central velocity dispersion* ($\log(\sigma_0)$), and is expressed mathematically with the following equation:

$$\log(r_e) = a \log(\sigma_0) + b \langle \mu \rangle_e + c \quad (1)$$

The FP relation is a direct consequence of the dynamical equilibrium condition (virial theorem) and of the regular behavior of both the mass-luminosity ratio and of the galactic structure of the ETGs along all the luminosity range. Due to its small intrinsic dispersion (~ 0.1 dex in r_e and σ_0 and ~ 0.1 mag in $\langle \mu \rangle_e$) the FP is considered a powerful tool in measuring galactic distances and also in studies of galactic formation and evolution (Kjærgaard, Jorgensen & Moles 1993; Jorgensen, Franx & Kjærgaard 1996; Jorgensen *et al.* 1999; Kelson *et al.* 1997).

A physically significant projection of the FP is the correlation between $\log(r_e)$ and $\langle \mu \rangle_e$, known as the Kormendy relation (KR):

$$\langle \mu \rangle_e = \alpha + \beta \log(r_e) \quad (2)$$

Several studies demonstrate that the ETGs in clusters define the KR with an intrinsic dispersion of approximately 0.4-mag in $\langle \mu \rangle_e$ (Hamabe & Kormendy 1987; Hoessel, Oegerle & Schneider 1987; Sandage & Peremulter 1991; Sandage & Lubin 2001; La Barbera *et al.* 2003). Recent studies show that low-density-environment ETGs and isolated ETGs also follow the KR with the same coefficients and intrinsic dispersion as do ETGs in

clusters (Reda *et al.* 2004; Nigoche-Netro *et al.* 2007). On the other hand, previous studies demonstrated that ETGs (plus bulges of spiral galaxies) formed two distinct families on the structural parameters plane; i.e. the family of bright ETGs ($M_B \leq -18$) that follows the KR and the family of dwarf ETGs ($M_B > -18$) with more disperse and heterogeneous properties (their effective parameters range over a wide interval for the same total luminosity) (Capaccioli, Caon & D’Onofrio 1992). Subsequently Graham & Guzmán (2003) showed that the difference between the bright elliptical (bright E) and the dwarf elliptical (dE) galaxies is only apparent and that there is a continuous structural relation between both classes. They say that the different behavior presented by the bright E and the dE galaxies in the $\log(r_e) - \langle \mu \rangle_e$ plane and the variations in the value of the slope of the relation do not imply a different formation mechanism, rather it may be interpreted as a systematic change in the shape of the light-profile with galactic magnitude (M). This, together with the fact that the intrinsic dispersion of the KR depends on the magnitude range (Nigoche-Netro *et al.* 2007) prompted us to study the behavior of the coefficients of the KR as functions of the magnitude range. If indeed, the values of the coefficients of the KR depend on the magnitude range within which the galaxies are contained, and this fact is not considered when performing comparisons of galaxy samples such as the dependence of the KR on the environment, on redshift or on wavelength, the differences which might be found may be misinterpreted.

In this paper, we present a compilation of 4 samples of ETGs which in total contain approximately 9400 galaxies and cover a relatively ample magnitude range ($\langle \Delta M \rangle \sim 6 - mag$). These samples correspond to photometric data from the literature and they are sufficiently large so that the results obtained may be considered as statistically significant. Using these data we analyze the behavior of the coefficients of the KR with respect to several characteristics of the magnitude range. We also present numerical simulations of the distribution of the galaxies on the $\log(r_e) - \langle \mu \rangle_e$ plane. These simulations allow us to

reproduce in a reasonable manner the results we obtain from the real samples of galaxies.

This paper is organized as follows. In section 2, we present the different samples used in the analysis of the KR. Section 3 describes the fitting method used in calculating the KR coefficients, as well as the behavior of the β coefficient with respect to the absolute magnitude range. Section 4 presents numerical simulations of the distribution of the galaxies on the $\log(r_e) - \langle \mu \rangle_e$ plane and finally in section 5 the conclusions are presented.

2. The samples

We use a Sloan Digital Sky Survey (SDSS) sample of 8666 ETGs (Bernardi *et al.* 2003) in filters g^* , r^* , i^* and z^* (absolute magnitude range $-18 \geq M_{g^*} > -24.1$ and its equivalent in other filters) as well as a sample of 626 ETGs in the Johnson V filter ($-16 \geq M_V > -22$) from 7 Abell clusters (WINGS project, Fasano *et al.* 2002; Fasano *et al.* 2004), a sample in filter Gunn r ($-17 \geq M_{Gr} > -24$) with 196 ETGs from the Coma cluster (Milvang-Jensen 1997; Aguerri *et al.* 2005) and a 54 ETGs sample in the filter Gunn r ($-18 \geq M_{Gr} > -22$) from the Hydra cluster (Milvang-Jensen 1997).

All the samples are redshift-homogeneous, except for the SDSS sample which cover a relatively ample redshift interval ($0.01 \leq z \leq 0.3$). It is important to say that for this sample, and due to the Malquist bias, those galaxies that are further away from us are also the brightest ones, so the few faint galaxies found in this sample have, in general, low redshifts. In Table 1 we present relevant information (number of galaxies, magnitude range and redshift) for the samples of galaxies we use in this paper. The magnitude range information is given in relation to the different filters used (from the literature) and also the approximate range for the B-magnitude (calculated by us). The transformation to the B filter was accomplished by use of the following equations: B - Gunn

$r = 1.15$ (Milvang-Jensen 1997) and $B - V = 0.92$ (Michard 2000). The filters g^* , r^* , i^* and z^* correspond approximately to the Johnson-Morgan-Cousins filters B, V, R_c and I_c respectively (Fukugita *et al.* 1996).

All the samples consider the photometric parameters $\log(r_e)$ and $\langle \mu \rangle_e$ corrected for different biases (galactic extinction, K correction and cosmological dimming). These parameters as well as their uncertainties were taken directly from the different papers cited above, except for the parameters for the Abell samples which constitute a private communication from the WINGS project team (Fasano *et al.* 2002; Fasano *et al.* 2004), and those for Coma (data from Aguerri *et al.* 2005). In this last case, given that Aguerri *et al.* (2005) give information for effective surface brightness (μ_e) instead of effective mean surface brightness ($\langle \mu \rangle_e$), we transform these data by using the following expression:

$$\langle \mu \rangle_e = \mu_e - F(n) \tag{3}$$

Where $F(n)$ is a function of the Sersic n -index (Graham & Driver 2005).

Finally, these photometric parameters (according to the papers where the samples were taken from), were obtained from the whole galaxy in the case of bright Es, and from the bulge in the case of bright S0s. For dwarf galaxies we follow the same procedure: information from the whole galaxy for the dEs and from the bulge for the dS0s.

EDITOR: PLACE TABLE 1 HERE.

3. Kormendy relation

3.1. Calculation of the Kormendy relation

The estimation of the KR coefficients may be severely affected by the fitting method and by the choice of dependent variable. The biases may be larger if there are measurement errors in the variables, if these errors are correlated and/or if there is intrinsic dispersion. The *Bivariate Correlated Errors and Intrinsic Scatter bisector* ($BCES_{Bis}$) fit (Isobe *et al.* 1990; Akritas & Bershady 1996) is a statistical model that takes into account the different sources of bias mentioned above, which are precisely those that affect our samples. In this work we use the $BCES_{Bis}$ method for the determination of the KR coefficients.

From the photometric parameters of the different galaxy samples, we calculate the coefficients of the KR in different magnitude ranges, the uncertainties of the coefficients, the correlation coefficient (Pearson Statistics) and the intrinsic dispersion of the KR (subtracting in quadrature from the intrinsic dispersion in $\langle \mu \rangle_e$ the residues dispersion due to the measurement errors of $\langle \mu \rangle_e$ and $\log(r_e)$) (see La Barbera *et al.* 2003). According to La Barbera *et al.* (2003), for the calculation of the intrinsic dispersion it is necessary to have the measurement errors in $\langle \mu \rangle_e$ and $\log(r_e)$, these errors come directly from the papers from which we take the galaxy samples (see section 2), while the errors in the KR coefficients were calculated by us following Akritas & Bershady (1996) in 1σ intervals. It is important to mention that the KR coefficients were calculated both in increasing magnitude intervals, as well as in narrow magnitude intervals. This allows us, among other things, to characterize the behavior of the KR coefficients with respect to the width of the magnitude range and the brightness of galaxies within the magnitude range so the results obtained may be utilized as reference for other studies in which different magnitude ranges are used. In Tables 2-5 we present the results for the values of the coefficients of the KR for the different samples of galaxies and for different magnitude

intervals.

EDITOR: PLACE TABLE 2 HERE.

EDITOR: PLACE TABLE 3 HERE.

EDITOR: PLACE TABLE 4 HERE.

EDITOR: PLACE TABLE 5 HERE.

3.2. Behavior of the Kormendy relation coefficients with respect to absolute magnitude range

From the analysis of the data for our different samples we notice that the intrinsic dispersion of the KR (σ_{KR}), as clearly stated by Nigoche-Netro *et al.* (2007), changes appreciably each time we include brighter galaxies in the samples, that is to say when we use increasing magnitude intervals (see Table 2). We also notice that the correlation coefficient (R) for each fit diminishes considerably. Apart from these changes, we can also see changes in the coefficients of the KR and that these changes are larger than the associated errors for most of the cases. The distribution of the β coefficient may be seen on Fig. 1, where it is interesting to note that this distribution presents a maximum at $M_B \sim -18 \pm 1$. On the other hand, we also perform the analysis of the data using magnitude intervals that are narrow (see Tables 3, 4 and 5), that is, not making samples which include each time brighter galaxies but considering galaxy samples in magnitude intervals of the same width

and progressively brighter (the case for magnitude intervals narrower than 1 magnitude can only be carried out for the SDSS samples due to the fact that these samples have a very large number of galaxies). For this case we can also see changes in the coefficients of the KR, however, the changes are less pronounced but still larger than the associated errors for most of the cases. It is interesting to note that for increasingly narrow magnitude intervals the values of the β coefficient show a maximum at $M_B \sim -18 \pm 1$, and that the β values tend to have values closer to 5 (see β values of SDSS sample on Figs. 2, 3 and 4). It is also important to point out that the intrinsic dispersion of the KR is relatively low in all cases, and that the correlation coefficient is, on the average superior to 0.9. The variation of the β coefficient when we consider narrow magnitude intervals may be seen on Figs. 2, 3 and 4 where a dependence between the β coefficient and absolute magnitude appears to be hinted at (mainly when we choose magnitude intervals with widths $\Delta M \geq 0.5 - mag$). However, it may be possible for the β coefficient to be constant ($\beta = 5$) and that the differences we find are the result of statistical fluctuations.

EDITOR: PLACE FIGURE 1 HERE.

EDITOR: PLACE FIGURE 2 HERE.

EDITOR: PLACE FIGURE 3 HERE.

EDITOR: PLACE FIGURE 4 HERE.

The question that β be constant and equal to 5 comes from the definition of absolute magnitude in terms of effective radius and effective mean surface brightness, that is:

$$M = \langle \mu \rangle_e - 5 \log(R_e) - 2.5 \log(2\pi) - 5 \log(D) + 5 \quad (4)$$

where R_e [arcsec] and D [pc] represent the effective radius and the distance to the object in question respectively and $\langle \mu \rangle_e$ [mag/arcsec²] is the effective mean surface brightness.

If we consider the effective radius in kiloparsecs (r_e) and a constant magnitude, we obtain the KR as follows:

$$\langle \mu \rangle_e = \alpha + 5 \log(r_e) \quad (5)$$

Which implies that

$$\beta = 5 \quad (6)$$

However, the observational data for β seem to move away from the expected value (mainly when $\Delta M \geq 0.5 - mag$). In order to clear this point, it is necessary to apply non-parametric tests to make certain that the fluctuations in the values of the slope are not products of chance variations.

3.3. Hypothesis Tests for the evaluation of β data

There are several non-parametric methods for the evaluation of sets of data (see Bendat & Piersol 1966). One of the most popular is the chi-square test. This test measures the discrepancy between an observed probability density and a theoretical probability density (i.e. a normal distribution). Another important test, which does not *a priori* assume a specific distribution, is that known as run test. There is one particularly interesting

non-parametric test (mean value test), which helps in finding out whether the data in question are distributed at random around a given value or whether this distribution is not a random one.

In Table 6 we show the results of the application of the tests to the different galaxy samples in narrow magnitude intervals. The null hypothesis of the mean value test (test 1) is that β has a normal distribution and that its mean value is 5 (we consider the data to have a measurement error equal to 10%), the null hypothesis of the run test (test 2) is that there is not an underlying trend in the β data and finally the null hypothesis of the chi-square test (test 3) is that the β data are random and that they follow a normal distribution. The percentages given in Table 6 refer to the confidence level with which we can reject the null hypothesis.

From Table 6 we can see that, on average, the null hypothesis may be rejected with a level of confidence of 95 %. This implies that there are strong reasons to believe that the mean value of β is not 5, that there is an underlying trend in the values of β and that the distribution of these values is not normal.

As we see in the previous paragraph, the applied tests to the different samples ($\Delta M \geq 0.5 - mag$) show that there are strong reasons to believe that the β -data are not distributed randomly around 5 and that there is an underlying trend. Moreover, when the magnitude intervals are increasingly narrower, there is an underlying trend for the values of the β coefficient (maximum at $M_B \sim -18 \pm 1$), but its values are ever closer to 5. From these results there are a number of questions that arise: Why is there an underlying trend in the values of β when we consider narrow magnitude intervals?, Why does this trend show a maximum at absolute magnitude $M_B \sim -18$?, and finally, Why do the values of β , in narrower magnitude intervals, keep on having an underlying trend even though their values are closer to 5? A possible answer to these questions is that the change in the value of the

slope might be due to the fact that the distribution of the galaxies on the $\log(r_e) - \langle \mu \rangle_e$ plane depends on the luminosity (Fig. 5, see further details in Varela 2004; D’Onofrio *et al.* 2006; Nigoche-Netro *et al.* 2007). It could also be due to the geometrical shape of the galaxy distribution on this plane. If the distribution of galaxies takes a rectangular shape, fitting a straight line to these data will produce different results from a straight-line fit to a galaxy distribution that takes a triangular shape or any other shape. In the following section we present numerical simulations of the galaxy distribution on the $\log(r_e) - \langle \mu \rangle_e$ plane that elucidate clearly the effects that the shape of the distribution of galaxies on this plane has over the values of the coefficients of the KR.

EDITOR: PLACE FIGURE 5 HERE.

4. Numerical simulations

To investigate whether the magnitude dependence of the KR coefficients is due to the geometric shape of the distribution of galaxies on the $\log(r_e) - \langle \mu \rangle_e$ plane (geometrical effect), we perform numerical simulations for each one of our samples of galaxies (Fig. 6). The simulations consist in giving values to $\log(r_e)$ in a similar radii range as that of the sample in question, fixing the faintest zero-point (α_0) of this sample (it is equivalent to fixing a magnitude) and fixing a slope of 5 (expected slope considering the definition of total absolute magnitude). Then, we take the same range of $\log(r_e)$, a α_0 slightly brighter (we take increments of 0.1 *mag*) and the same slope of 5, and so on until we cover the whole range of brightness of the sample in question. The resulting data distribution consists in parallel lines of slope 5 which shift to brighter magnitude. Once the data are generated, we simulate the observed depopulation effect on the upper region of the galaxy distribution (Fig. 7). This depopulation is known as the exclusion zone (Bender, Burstein & Faber

1992) and may be characterized by a straight line (Line of Avoidance or LOA) that has a slope approximately equal to 2.7 (D’Onofrio *et al.* 2006). Since we do not know the way in which galaxies locations in the lower part of the $\log(r_e) - \langle \mu \rangle_e$ plane behave, we consider the following 3 cases in the simulation of this region:

Case 1. It consists in setting a fixed limit-radius for all the magnitude intervals, so that the galaxies are contained within a triangle, one of whose sides is parallel to the $\langle \mu \rangle_e$ axis.

Case 2. In this case we consider that the lower region of the diagram is limited by a 2.7-slope straight line, that is, there is an identical exclusion zone in this part of the diagram, as that observed in the upper part. Therefore the galaxies appear to be contained within a parallelogram and their distribution appears to be symmetric with respect to an axis that contains the barycenter of the galaxy distribution and is parallel to the $\log(r_e)$ axis, we shall call this axis from now on the X_{Bright} -axis. Further details on the definition of the X_{Bright} -axis, as well as on the symmetry type discussed here, are given in Fig. 8.

Case 3. We consider the lower region as limited in brightness, so galaxies are contained within a triangle with one of its sides parallel to the $\log(r_e)$ axis.

EDITOR: PLACE FIGURE 6 HERE.

EDITOR: PLACE FIGURE 7 HERE.

EDITOR: PLACE FIGURE 8 HERE.

EDITOR: PLACE TABLE 7 HERE.

EDITOR: PLACE TABLE 8 HERE.

The results of the analysis of the KR show that when we consider increasing magnitude intervals (Table 7), there are slope changes in all the cases, and these changes are always larger than the errors. We also find that the geometric shape of the distribution of galaxies changes each time we include brighter galaxies in the samples (Fig. 7). On the other hand, when we consider narrow 1-magnitude intervals (Table 8), there are also slope changes (except for case 2), however, the changes are less pronounced but still larger than the errors and if the magnitude intervals are progressively narrower, then the changes diminish considerably getting ever closer to the value of 5, just as it occurs for the real samples. Finally, if the magnitude interval is equal to 0.1-*mag* then the slope is exactly equal to 5 since that is the way we define the samples.

It is important to mention that when we consider narrow magnitude intervals we are able to reproduce, in a reasonable manner, the β coefficient variations and the underlying trend (maximum at $M_B \sim -18 \pm 1$) found for the real samples (except for case 2) (Fig. 9). We also find that the geometric shape of the distribution of galaxies changes systematically when we consider brighter magnitude intervals (except for case 2) (Fig. 7). We must remind the reader that Case 2 corresponds to a symmetrical galaxy distribution over the $\log(r_e) - \langle \mu \rangle_e$ plane.

Moreover, we find that both the zero point (α) and the intrinsic dispersion (σ_{KR}) of KR change systematically when we consider brighter galaxies. This latter result confirms the dependence of the intrinsic dispersion with the magnitude range as reported in Nigoche-Netro et al. 2007.

From the aforementioned, we may infer that the KR coefficients and its intrinsic dispersion depend on the width and brightness of the magnitude range. This dependence is

caused by a geometrical effect due to the fact that the distribution of the galaxies on the $\log(r_e) - \langle \mu \rangle_e$ plane depends on luminosity and also to the fact that this distribution is not symmetrical with respect to the X_{bright} -axis, in other words, the geometric shape of the distribution of galaxies on the $\log(r_e) - \langle \mu \rangle_e$ plane changes systematically as we consider brighter galaxies, and so the values of the KR coefficients change too, because the fitting of a straight line to a set of data does not give the same result for slope and intercept values for data distributed with a rectangular shape as for data distributed with a triangular shape or, for that matter, with another geometrical shape.

EDITOR: PLACE FIGURE 9 HERE.

5. Conclusions

We have compiled 4 samples of ETGs with information for their photometric parameters $\log(r_e)$ and $\langle \mu \rangle_e$, these samples contain a total of ~ 9400 galaxies in a relatively ample magnitude range ($\langle \Delta M \rangle \sim 6.0 - mag$). From the values of their photometric parameters, we have made an analysis of the behavior of the coefficients and intrinsic dispersion of the KR with respect to several characteristics of the magnitude range within which the galaxies are contained. The results from this study are presented as follows:

- We find that when we include in the samples galaxies which get progressively brighter (increasing magnitude intervals) or if we consider galaxy samples in progressively brighter fixed-width magnitude intervals (narrow magnitude intervals), the KR coefficients change and these changes result to be larger than the associated errors for most of the cases. We also find that the distribution of the values of the β coefficient both in increasing and narrow magnitude intervals shows a maximum at

$M_B \sim -18 \pm 1$. We perform non-parametric tests on the β coefficient data and they indicate that the variations are real and that there is evidence of an underlying trend, that is, there is evidence that the β coefficient changes systematically when we consider brighter galaxies and that the value of this coefficient attains a maximum value at $M_B \sim -18 \pm 1$ and smaller values at the extremes of the magnitude spectrum available.

- We find that when the magnitude intervals are increasingly narrower, there is also an underlying trend for the values of the β coefficient (maximum at $M_B \sim -18 \pm 1$), but its values are ever closer to 5 (expected value from the definition of absolute magnitude). It is important to note that the fact that the value of the β coefficient tends to 5 for very narrow magnitude intervals might imply that the variation of β is not dependent on the absolute magnitude but rather on the absolute magnitude range within which the galaxies are contained.

In order to elucidate this last point, we perform numerical simulations of the different samples of galaxies under study. The results of the analysis of the variation of the KR coefficients, both in increasing and in narrow magnitude intervals show that the coefficients depend on the width and brightness of the magnitude range and that this dependence comes as a result of a geometrical effect due to the fact that:

- The distribution of galaxies on the $\log(r_e) - \langle \mu \rangle_e$ plane depends on luminosity, and
 - That the geometric shape of the distribution of the galaxies on this plane is not symmetrical (see Sect. 4 for full details).
- Finally, numerical simulations confirm the fact that the intrinsic dispersion of the KR depends on the magnitude range, as asserted in Nigoche-Netro *et al.* (2007).

From the previously mentioned results, it is very important to establish that if the magnitude range is not taken into consideration when performing comparisons of galaxy samples such as the dependence of the KR on the environment, on redshift or on wavelength, the differences which might be found may be misinterpreted.

We would like to thank Project WINGS (Fasano *et al.* 2002; Fasano *et al.* 2004) for providing the photometric parameters for the samples in 7 Abell clusters, Consejo Nacional de Ciencia y Tecnología (México) for a PhD fellowship number 132526, Ministerio Español de Educación y Ciencia for grant PNAYA2006, Instituto de Matemáticas y Física Fundamental (CSIC, España) and Instituto de Astronomía (UNAM, México) for all the facilities provided for the realization of this project.

Table 1. Name, Number of galaxies, Magnitude range (according to the papers where the samples were taken from), Approximate magnitude range in the B-Filter (calculated by us) and redshift of the different galaxy samples compiled in this work. In the 7 Abell cluster sample we include the following clusters: A147, A168, A193, A2457, A2589, A2593, and A2626.

Sample	N	Magnitude range	Approximate magnitude range in the B-filter	z
7 Abell clusters (V filter)	626	$-16.0 \geq M_V > -22.0$	$-15.1 \geq M_B > -21.1$	0.048
Coma cluster (Gunn r filter)	196	$-17.0 \geq M_{Gr} > -24.0$	$-15.9 \geq M_B > -22.9$	0.024
Hydra cluster (Gunn r filter)	54	$-18.0 \geq M_{Gr} > -22.0$	$-16.9 \geq M_B > -20.9$	0.014
SDSS (g* filter)	8666	$-18.0 \geq M_{g^*} > -24.1$	$-18.0 \geq M_B > -24.1$	≤ 0.3
SDSS (r* filter)	8666	$-18.6 \geq M_{r^*} > -24.7$	$-18.0 \geq M_B > -24.1$	≤ 0.3
SDSS (i* filter)	8666	$-19.0 \geq M_{i^*} > -25.1$	$-18.0 \geq M_B > -24.1$	≤ 0.3
SDSS (z* filter)	8666	$-19.3 \geq M_{z^*} > -25.3$	$-18.0 \geq M_B > -24.1$	≤ 0.3

Table 2. KR coefficients for the different galaxy samples in increasing intervals of magnitude. MI is the absolute magnitude interval within which the galaxies are distributed, N is the number of galaxies in the magnitude interval, α_{Bis} is the zero point of KR, β_{Bis} is the slope of KR, σ_{KR} is the intrinsic dispersion of KR and R is the correlation coefficient of the fit (Pearson Statistics).

MI	N	α_{Bis}	β_{Bis}	σ_{KR}	R	MI	N	α_{Bis}	β_{Bis}	σ_{KR}	R
Abell (V)						Coma (Gunn r)					
-16 $\geq M >$ -17	136	21.997 \pm 0.063	4.733 \pm 0.268	0.201	0.933	-17 $\geq M >$ -18	17	20.019 \pm 0.138	2.537 \pm 0.276	0.536	0.802
-16 $\geq M >$ -18	284	21.232 \pm 0.075	5.949 \pm 0.274	0.488	0.834	-17 $\geq M >$ -19	68	19.377 \pm 0.111	3.266 \pm 0.313	0.692	0.705
-16 $\geq M >$ -19	394	20.917 \pm 0.116	5.721 \pm 0.411	0.719	0.715	-17 $\geq M >$ -20	82	19.302 \pm 0.095	3.281 \pm 0.229	0.667	0.769
-16 $\geq M >$ -20	519	20.574 \pm 0.190	5.216 \pm 0.630	1.031	0.504	-17 $\geq M >$ -21	109	19.135 \pm 0.093	3.210 \pm 0.219	0.656	0.743
-16 $\geq M >$ -21	593	20.967 \pm 0.216	3.102 \pm 0.673	1.143	0.326	-17 $\geq M >$ -22	169	18.917 \pm 0.090	2.982 \pm 0.167	0.674	0.725
-16 $\geq M >$ -22	626	21.229 \pm 0.155	2.070 \pm 0.445	1.143	0.251	-17 $\geq M >$ -23	192	18.824 \pm 0.092	2.687 \pm 0.173	0.711	0.645
-16 $\geq M >$ -23	-17 $\geq M >$ -24	196	18.837 \pm 0.089	2.598 \pm 0.158	0.708	0.651
Hydra (Gunn r)											
-18 $\geq M >$ -19	4	19.722 \pm 0.024	5.037 \pm 0.062	0.077	0.996						
-18 $\geq M >$ -20	15	18.964 \pm 0.122	5.721 \pm 0.158	0.378	0.961						
-18 $\geq M >$ -21	42	18.295 \pm 0.151	5.277 \pm 0.213	0.685	0.885						
-18 $\geq M >$ -22	54	18.068 \pm 0.170	5.097 \pm 0.256	0.824	0.813						
SDSS (g*)						SDSS (r*)					
-18.5 $\geq M >$ -19	26	18.392 \pm 0.040	4.808 \pm 0.100	0.128	0.982	-18.5 $\geq M >$ -19	3	18.332 \pm 0.070	5.098 \pm 0.727	0.170	0.853
-18.5 $\geq M >$ -20	517	18.978 \pm 0.027	4.726 \pm 0.057	0.297	0.900	-18.5 $\geq M >$ -20	77	18.962 \pm 0.051	4.645 \pm 0.138	0.258	0.929
-18.5 $\geq M >$ -21	2856	18.686 \pm 0.020	3.909 \pm 0.033	0.362	0.825	-18.5 $\geq M >$ -21	1014	18.204 \pm 0.025	4.356 \pm 0.050	0.322	0.877
-18.5 $\geq M >$ -22	6687	18.790 \pm 0.016	3.057 \pm 0.021	0.406	0.763	-18.5 $\geq M >$ -22	4057	17.963 \pm 0.019	3.609 \pm 0.030	0.386	0.784
-18.5 $\geq M >$ -23	8516	18.949 \pm 0.014	2.641 \pm 0.016	0.425	0.744	-18.5 $\geq M >$ -23	7646	18.093 \pm 0.015	2.858 \pm 0.020	0.418	0.724
-18.5 $\geq M >$ -24	8661	18.989 \pm 0.013	2.572 \pm 0.015	0.425	0.749	-18.5 $\geq M >$ -24	8630	18.214 \pm 0.013	2.572 \pm 0.017	0.426	0.717
-18.5 $\geq M >$ -25	-18.5 $\geq M >$ -25	8666	18.225 \pm 0.013	2.552 \pm 0.016	0.426	0.721
SDSS (i*)						SDSS (z*)					
-19 $\geq M >$ -20	31	17.458 \pm 0.059	4.717 \pm 0.209	0.219	0.937	-19.5 $\geq M >$ -19	15	17.331 \pm 0.038	4.482 \pm 0.104	0.116	0.984
-19 $\geq M >$ -21	505	18.033 \pm 0.027	4.540 \pm 0.062	0.311	0.894	-19.5 $\geq M >$ -20	210	17.940 \pm 0.035	4.742 \pm 0.085	0.299	0.908
-19 $\geq M >$ -22	2805	17.605 \pm 0.020	3.941 \pm 0.036	0.371	0.816	-19.5 $\geq M >$ -21	1799	17.312 \pm 0.022	4.259 \pm 0.042	0.358	0.850
-19 $\geq M >$ -23	6645	17.663 \pm 0.015	3.047 \pm 0.022	0.406	0.741	-19.5 $\geq M >$ -22	5440	17.264 \pm 0.017	3.309 \pm 0.025	0.400	0.765
-19 $\geq M >$ -24	8512	17.808 \pm 0.013	2.598 \pm 0.013	0.422	0.716	-19.5 $\geq M >$ -23	8277	17.437 \pm 0.013	2.680 \pm 0.017	0.414	0.738
-19 $\geq M >$ -25	8664	17.843 \pm 0.012	2.529 \pm 0.016	0.422	0.723	-19.5 $\geq M >$ -24	8658	17.504 \pm 0.012	2.543 \pm 0.015	0.413	0.748
-19 $\geq M >$ -26	-19.5 $\geq M >$ -25	8665	17.507 \pm 0.012	2.537 \pm 0.015	0.413	0.750

Table 3. KR coefficients for the different galaxy samples in narrow 1 – *mag* intervals. MI is the absolute magnitude interval within which the galaxies are distributed, N is the number of galaxies in the magnitude interval, α_{Bis} is the zero point of KR, β_{Bis} is the slope of KR, σ_{KR} is the intrinsic dispersion of KR and R is the correlation coefficient of the fit (Pearson Statistics).

MI	N	α_{Bis}	β_{Bis}	σ_{KR}	R	MI	N	α_{Bis}	β_{Bis}	σ_{KR}	R
Abell (V)						Coma (Gunn r)					
-16.0 $\geq M >$ -17.0	136	21.997 \pm 0.063	4.733 \pm 0.268	0.201	0.933	-17.0 $\geq M >$ -18.0	17	20.019 \pm 0.138	2.537 \pm 0.276	0.536	0.802
-17.0 $\geq M >$ -18.0	148	21.009 \pm 0.051	5.276 \pm 0.193	0.275	0.924	-18.0 $\geq M >$ -19.0	51	19.087 \pm 0.111	3.783 \pm 0.256	0.623	0.772
-18.0 $\geq M >$ -19.0	110	20.223 \pm 0.082	4.886 \pm 0.319	0.310	0.918	-19.0 $\geq M >$ -20.0	14	18.957 \pm 0.081	3.243 \pm 0.090	0.316	0.970
-19.0 $\geq M >$ -20.0	125	19.128 \pm 0.044	4.983 \pm 0.093	0.287	0.929	-20.0 $\geq M >$ -21.0	27	18.015 \pm 0.044	4.839 \pm 0.077	0.182	0.971
-20.0 $\geq M >$ -21.0	74	18.310 \pm 0.070	4.791 \pm 0.120	0.289	0.926	-21.0 $\geq M >$ -22.0	51	17.427 \pm 0.052	4.685 \pm 0.067	0.251	0.965
-21.0 $\geq M >$ -22.0	33	18.246 \pm 0.071	3.830 \pm 0.072	0.146	0.941	-22.0 $\geq M >$ -23.0	32	16.879 \pm 0.035	4.512 \pm 0.156	0.221	0.936
-22.0 $\geq M >$ -23.0	-23.0 $\geq M >$ -24.0	4	17.087 \pm 0.057	3.569 \pm 0.211	0.243	0.894
Hydra (Gunn r)											
-18.0 $\geq M >$ -19.0	4	19.722 \pm 0.024	5.037 \pm 0.062	0.077	0.996						
-19.0 $\geq M >$ -20.0	11	18.994 \pm 0.115	5.255 \pm 0.167	0.312	0.968						
-20.0 $\geq M >$ -21.0	27	17.902 \pm 0.063	5.127 \pm 0.078	0.237	0.987						
-21.0 $\geq M >$ -22.0	12	17.142 \pm 0.112	4.821 \pm 0.148	0.240	0.974						
SDSS (g*)						SDSS (r*)					
-19.0 $\geq M >$ -20.0	491	18.922 \pm 0.021	4.760 \pm 0.044	0.238	0.936	-19.0 $\geq M >$ -20.0	74	18.864 \pm 0.035	4.966 \pm 0.091	0.220	0.948
-20.0 $\geq M >$ -21.0	2339	18.254 \pm 0.013	4.463 \pm 0.021	0.249	0.918	-20.0 $\geq M >$ -21.0	937	18.036 \pm 0.014	4.619 \pm 0.028	0.233	0.937
-21.0 $\geq M >$ -22.0	3831	17.590 \pm 0.014	4.277 \pm 0.017	0.245	0.912	-21.0 $\geq M >$ -22.0	3043	17.366 \pm 0.011	4.342 \pm 0.018	0.244	0.914
-22.0 $\geq M >$ -23.0	1829	16.874 \pm 0.023	4.279 \pm 0.023	0.223	0.927	-22.0 $\geq M >$ -23.0	3589	16.624 \pm 0.014	4.320 \pm 0.017	0.242	0.905
-23.0 $\geq M >$ -24.0	145	16.386 \pm 0.086	4.118 \pm 0.072	0.161	0.951	-23.0 $\geq M >$ -24.0	984	16.016 \pm 0.027	4.224 \pm 0.028	0.199	0.934
-24.0 $\geq M >$ -25.0	-24.0 $\geq M >$ -25.0	36	15.474 \pm 0.162	4.162 \pm 0.132	0.151	0.953
SDSS (i*)						SDSS (z*)					
-19.0 $\geq M >$ -20.0	31	17.458 \pm 0.059	4.717 \pm 0.209	0.219	0.937	-19.0 $\geq M >$ -20.0
-20.0 $\geq M >$ -21.0	474	17.926 \pm 0.018	4.713 \pm 0.039	0.235	0.941	-20.0 $\geq M >$ -21.0	195	17.859 \pm 0.024	4.838 \pm 0.056	0.229	0.986
-21.0 $\geq M >$ -22.0	2300	17.213 \pm 0.012	4.481 \pm 0.021	0.249	0.918	-21.0 $\geq M >$ -22.0	1589	17.065 \pm 0.013	4.610 \pm 0.024	0.246	0.980
-22.0 $\geq M >$ -23.0	3840	16.572 \pm 0.012	4.250 \pm 0.016	0.241	0.904	-22.0 $\geq M >$ -23.0	3641	16.475 \pm 0.011	4.213 \pm 0.015	0.236	0.980
-23.0 $\geq M >$ -24.0	1867	15.877 \pm 0.020	4.239 \pm 0.023	0.219	0.918	-23.0 $\geq M >$ -24.0	2837	15.831 \pm 0.015	4.142 \pm 0.018	0.223	0.977
-24.0 $\geq M >$ -25.0	152	15.212 \pm 0.068	4.240 \pm 0.062	0.160	0.956	-24.0 $\geq M >$ -25.0	381	15.308 \pm 0.035	4.027 \pm 0.033	0.158	0.973

Table 4. KR coefficients for the SDSS galaxy samples in narrow $0.5 - mag$ intervals. MI is the absolute magnitude interval within which the galaxies are distributed, N is the number of galaxies in the magnitude interval, α_{Bis} is the zero point of KR, β_{Bis} is the slope of KR, σ_{KR} is the intrinsic dispersion of KR and R is the correlation coefficient of the fit (Pearson Statistics).

MI	N	α_{Bis}	β_{Bis}	σ_{KR}	R	MI	N	α_{Bis}	β_{Bis}	σ_{KR}	R
SDSS (g*)						SDSS (r*)					
$-18.5 \geq M > -19.0$	26	18.392 ± 0.040	4.808 ± 0.100	0.128	0.982	$-19.0 \geq M > -19.5$	14	17.884 ± 0.025	4.747 ± 0.124	0.090	0.981
$-19.0 \geq M > -19.5$	101	19.270 ± 0.020	4.913 ± 0.041	0.141	0.983	$-19.5 \geq M > -20.0$	60	18.781 ± 0.024	4.952 ± 0.063	0.139	0.982
$-19.5 \geq M > -20.0$	390	18.760 ± 0.012	4.923 ± 0.025	0.136	0.978	$-20.0 \geq M > -20.5$	229	18.253 ± 0.014	5.007 ± 0.033	0.141	0.980
$-20.0 \geq M > -20.5$	898	18.317 ± 0.010	4.883 ± 0.018	0.139	0.976	$-20.5 \geq M > -21.0$	707	17.842 ± 0.001	4.826 ± 0.019	0.135	0.978
$-20.5 \geq M > -21.0$	1441	17.902 ± 0.001	4.778 ± 0.014	0.140	0.974	$-21.0 \geq M > -21.5$	1230	17.357 ± 0.001	4.850 ± 0.015	0.137	0.976
$-21.0 \geq M > -21.5$	1899	17.475 ± 0.001	4.725 ± 0.012	0.134	0.973	$-21.5 \geq M > -22.0$	1813	16.926 ± 0.001	4.773 ± 0.013	0.136	0.973
$-21.5 \geq M > -22.0$	1932	16.947 ± 0.012	4.800 ± 0.013	0.138	0.973	$-22.0 \geq M > -22.5$	1995	16.439 ± 0.010	4.807 ± 0.130	0.140	0.969
$-22.0 \geq M > -22.5$	1308	15.182 ± 0.015	4.706 ± 0.015	0.137	0.972	$-22.5 \geq M > -23.0$	1594	14.605 ± 0.013	4.785 ± 0.014	0.136	0.970
$-22.5 \geq M > -23.0$	521	16.116 ± 0.028	4.714 ± 0.025	0.140	0.975	$-23.0 \geq M > -23.5$	762	15.576 ± 0.020	4.755 ± 0.021	0.132	0.971
$-23.0 \geq M > -23.5$	129	15.835 ± 0.059	4.587 ± 0.048	0.124	0.971	$-23.5 \geq M > -24.0$	222	15.295 ± 0.035	4.615 ± 0.033	0.118	0.973
$-23.5 \geq M > -24.0$	16	16.859 ± 0.179	3.593 ± 0.125	0.098	0.952	$-24.0 \geq M > -24.5$	31	14.930 ± 0.104	4.608 ± 0.085	0.097	0.981
$-24.0 \geq M > -24.5$	$-24.5 \geq M > -25.0$	5	14.261 ± 0.101	4.784 ± 0.079	0.059	0.985
SDSS (i*)						SDSS (z*)					
$-19.0 \geq M > -19.5$	4	17.876 ± 0.065	4.769 ± 0.229	0.131	0.973	$-19.5 \geq M > -20.0$	15	17.331 ± 0.038	4.482 ± 0.104	0.116	0.984
$-19.5 \geq M > -20.0$	27	18.713 ± 0.038	5.202 ± 0.133	0.151	0.970	$-20.0 \geq M > -20.5$	39	18.220 ± 0.022	4.924 ± 0.055	0.112	0.986
$-20.0 \geq M > -20.5$	102	18.267 ± 0.0190	4.880 ± 0.047	0.142	0.979	$-20.5 \geq M > -21.0$	156	17.731 ± 0.016	4.963 ± 0.039	0.140	0.980
$-20.5 \geq M > -21.0$	372	17.791 ± 0.001	4.812 ± 0.022	0.129	0.982	$-21.0 \geq M > -21.5$	536	17.281 ± 0.001	4.819 ± 0.020	0.136	0.980
$-21.0 \geq M > -21.5$	855	17.329 ± 0.001	4.862 ± 0.018	0.136	0.977	$-21.5 \geq M > -22.0$	1056	16.801 ± 0.001	4.865 ± 0.016	0.139	0.977
$-21.5 \geq M > -22.0$	1445	16.912 ± 0.001	4.747 ± 0.014	0.138	0.975	$-22.0 \geq M > -22.5$	1658	16.403 ± 0.008	4.715 ± 0.013	0.136	0.973
$-22.0 \geq M > -22.5$	1906	16.457 ± 0.001	4.744 ± 0.014	0.135	0.970	$-22.5 \geq M > -23.0$	1988	15.934 ± 0.001	4.738 ± 0.013	0.135	0.970
$-22.5 \geq M > -23.0$	1934	14.551 ± 0.011	4.814 ± 0.013	0.138	0.969	$-23.0 \geq M > -23.5$	1790	14.113 ± 0.012	4.708 ± 0.014	0.135	0.968
$-23.0 \geq M > -23.5$	1343	15.557 ± 0.015	4.729 ± 0.017	0.135	0.968	$-23.5 \geq M > -24.0$	1042	15.122 ± 0.018	4.644 ± 0.019	0.132	0.967
$-23.5 \geq M > -24.0$	524	15.160 ± 0.021	4.674 ± 0.021	0.127	0.973	$-24.0 \geq M > -24.5$	311	14.894 ± 0.031	4.448 ± 0.028	0.117	0.971
$-24.0 \geq M > -24.5$	136	14.800 ± 0.047	4.624 ± 0.041	0.119	0.976	$-24.5 \geq M > -25.0$	67	14.483 ± 0.079	4.495 ± 0.066	0.103	0.976
$-24.5 \geq M > -25.0$	16	14.718 ± 0.153	4.373 ± 0.122	0.110	0.955	$-25.0 \geq M > -25.5$	7	14.818 ± 0.408	3.962 ± 0.272	0.076	0.921

Table 5. KR coefficients for the SDSS galaxy samples in narrow 0.25 – *mag* intervals. MI is the absolute magnitude interval within which the galaxies are distributed, N is the number of galaxies in the magnitude interval, α_{Bis} is the zero point of KR, β_{Bis} is the slope of KR, σ_{KR} is the intrinsic dispersion of KR and R is the correlation coefficient of the fit (Pearson Statistics).

MI	N	α_{Bis}	β_{Bis}	σ_{KR}	R	MI	N	α_{Bis}	β_{Bis}	σ_{KR}	R
SDSS (g*)						SDSS (r*)					
-18.50 $\geq M >$ -18.75	10	19.905±0.023	4.910±0.122	0.059	0.993	-19.00 $\geq M >$ -19.25	3	17.879±0.014	5.660±0.173	0.050	0.985
-18.75 $\geq M >$ -19.00	16	19.642±0.023	5.002±0.049	0.062	0.996	-19.25 $\geq M >$ -19.50	11	19.231±0.024	4.823±0.014	0.067	0.990
-19.00 $\geq M >$ -19.25	37	19.448±0.016	4.851±0.044	0.067	0.993	-19.50 $\geq M >$ -19.75	24	18.902±0.019	5.077±0.053	0.075	0.994
-19.25 $\geq M >$ -19.50	65	19.156±0.012	4.973±0.023	0.068	0.996	-19.75 $\geq M >$ -20.00	36	18.657±0.016	5.064±0.051	0.073	0.993
-19.50 $\geq M >$ -19.75	124	18.898±0.001	5.014±0.022	0.069	0.994	-20.00 $\geq M >$ -20.25	83	18.404±0.11	5.040±0.025	0.072	0.993
-19.75 $\geq M >$ -20.00	266	17.257±0.001	5.000±0.018	0.071	0.994	-20.25 $\geq M >$ -20.50	147	18.178±0.001	4.951±0.021	0.073	0.994
-20.00 $\geq M >$ -20.25	375	18.432±0.001	4.942±0.014	0.070	0.994	-20.50 $\geq M >$ -20.75	295	17.935±0.001	4.945±0.016	0.069	0.994
-20.25 $\geq M >$ -20.50	523	18.169±0.001	4.972±0.012	0.071	0.993	-20.75 $\geq M >$ -21.00	412	16.291±0.001	4.959±0.012	0.068	0.993
-20.50 $\geq M >$ -20.75	682	17.940±0.001	4.938±0.010	0.073	0.993	-21.00 $\geq M >$ -21.25	542	17.421±0.001	4.994±0.012	0.071	0.993
-20.75 $\geq M >$ -21.00	761	17.693±0.001	4.930±0.010	0.068	0.993	-21.25 $\geq M >$ -21.50	690	17.204±0.001	4.942±0.011	0.072	0.992
-21.00 $\geq M >$ -21.25	937	17.467±0.001	4.903±0.009	0.072	0.992	-21.50 $\geq M >$ -21.75	842	16.947±0.001	4.948±0.010	0.072	0.992
-21.25 $\geq M >$ -21.50	964	17.209±0.001	4.928±0.009	0.072	0.992	-21.75 $\geq M >$ -22.00	975	16.722±0.001	4.919±0.009	0.071	0.992
-21.50 $\geq M >$ -21.75	985	15.561±0.001	4.932±0.009	0.071	0.993	-22.00 $\geq M >$ -22.25	995	16.466±0.001	4.934±0.010	0.074	0.992
-21.75 $\geq M >$ -22.00	948	16.699±0.001	4.945±0.010	0.073	0.991	-22.25 $\geq M >$ -22.50	998	16.203±0.001	4.955±0.009	0.072	0.993
-22.00 $\geq M >$ -22.25	740	16.480±0.011	4.914±0.012	0.070	0.992	-22.50 $\geq M >$ -22.75	885	14.563±0.001	4.958±0.010	0.070	0.992
-22.25 $\geq M >$ -22.50	564	16.187±0.014	4.961±0.013	0.078	0.990	-22.75 $\geq M >$ -23.00	711	15.744±0.010	4.921±0.011	0.071	0.992
-22.50 $\geq M >$ -22.75	329	16.007±0.017	4.897±0.016	0.072	0.992	-23.00 $\geq M >$ -23.25	475	15.478±0.014	4.945±0.015	0.069	0.993
-22.75 $\geq M >$ -23.00	191	15.733±0.025	4.915±0.022	0.076	0.992	-23.25 $\geq M >$ -23.50	282	15.294±0.018	4.886±0.017	0.070	0.992
-23.00 $\geq M >$ -23.25	93	15.585±0.045	4.838±0.038	0.065	0.989	-23.50 $\geq M >$ -23.75	158	15.008±0.027	4.926±0.025	0.069	0.990
-23.25 $\geq M >$ -23.50	35	13.940±0.084	4.845±0.065	0.073	0.989	-23.75 $\geq M >$ -24.00	63	14.789±0.045	4.910±0.036	0.062	0.992
-23.50 $\geq M >$ -23.75	11	15.635±0.215	4.490±0.163	0.067	0.975	-24.00 $\geq M >$ -24.25	25	14.677±0.062	4.834±0.047	0.050	0.990
-23.75 $\geq M >$ -24.00	-24.25 $\geq M >$ -24.50	6	11.992±0.187	5.593±0.142	0.038	0.963
-24.00 $\geq M >$ -24.25	-24.50 $\geq M >$ -24.75	5	14.261±0.101	4.784±0.079	0.059	0.985
SDSS (i*)						SDSS (z*)					
-19.25 $\geq M >$ -19.50	3	17.804±0.028	4.880±0.071	0.048	0.997	-19.50 $\geq M >$ -19.75	3	17.508±0.053	4.667±0.105	0.086	0.994
-19.50 $\geq M >$ -19.75	12	18.928±0.018	4.815±0.050	0.057	0.996	-19.75 $\geq M >$ -20.00	12	18.628±0.019	4.779±0.062	0.063	0.994
-19.75 $\geq M >$ -19.00	15	18.618±0.020	5.042±0.071	0.073	0.991	-20.00 $\geq M >$ -20.25	11	18.345±0.019	5.102±0.095	0.065	0.992
-20.00 $\geq M >$ -20.25	35	18.448±0.015	4.841±0.041	0.069	0.995	-20.25 $\geq M >$ -20.50	28	18.153±0.016	4.966±0.043	0.057	0.990
-20.25 $\geq M >$ -20.50	67	18.182±0.012	4.857±0.028	0.069	0.995	-20.50 $\geq M >$ -20.75	63	17.900±0.012	4.885±0.029	0.071	0.994
-20.50 $\geq M >$ -20.75	124	14.789±0.045	4.999±0.024	0.071	0.995	-20.75 $\geq M >$ -21.00	93	14.789±0.045	4.987±0.027	0.069	0.994
-20.75 $\geq M >$ -20.00	240	17.677±0.001	4.918±0.015	0.069	0.995	-21.00 $\geq M >$ -21.25	200	17.413±0.001	4.867±0.019	0.072	0.994
-21.00 $\geq M >$ -21.25	373	16.045±0.001	4.922±0.014	0.069	0.994	-21.25 $\geq M >$ -21.50	336	15.754±0.001	4.938±0.015	0.074	0.993
-21.25 $\geq M >$ -21.50	484	17.184±0.001	4.956±0.013	0.073	0.994	-21.50 $\geq M >$ -21.75	462	16.904±0.001	4.942±0.013	0.074	0.993
-21.50 $\geq M >$ -21.75	675	16.944±0.001	4.943±0.011	0.071	0.993	-21.75 $\geq M >$ -22.00	594	16.668±0.001	4.918±0.010	0.067	0.994
-21.75 $\geq M >$ -21.00	771	16.716±0.001	4.901±0.009	0.072	0.993	-22.00 $\geq M >$ -22.25	720	16.436±0.001	4.901±0.011	0.069	0.993
-22.00 $\geq M >$ -22.25	929	16.483±0.001	4.893±0.009	0.070	0.929	-22.25 $\geq M >$ -22.50	938	16.196±0.001	4.888±0.009	0.069	0.992
-22.25 $\geq M >$ -22.50	976	14.789±0.045	4.928±0.009	0.071	0.992	-22.50 $\geq M >$ -22.75	986	14.789±0.045	4.904±0.010	0.072	0.992
-22.50 $\geq M >$ -22.75	1018	15.948±0.001	4.962±0.010	0.072	0.991	-22.75 $\geq M >$ -23.00	1002	15.690±0.001	4.914±0.011	0.072	0.990
-22.75 $\geq M >$ -22.00	916	14.305±0.001	4.965±0.011	0.070	0.992	-23.00 $\geq M >$ -23.25	960	14.087±0.001	4.876±0.010	0.070	0.993
-23.00 $\geq M >$ -23.25	763	15.495±0.001	4.919±0.011	0.073	0.991	-23.25 $\geq M >$ -23.50	830	15.259±0.001	4.850±0.011	0.069	0.993
-23.25 $\geq M >$ -23.50	577	15.234±0.014	4.937±0.015	0.069	0.991	-23.50 $\geq M >$ -23.75	636	14.976±0.013	4.899±0.014	0.070	0.990
-23.50 $\geq M >$ -23.75	337	15.023±0.014	4.896±0.014	0.065	0.993	-23.75 $\geq M >$ -24.00	406	14.793±0.018	4.833±0.017	0.070	0.985

Table 6. Hypothesis Test for the evaluation of the β_{Bis} data from the different samples of galaxies. Tests 1, 2 and 3 correspond to the mean value, run and chi-square tests respectively. The null hypothesis of test 1 is that β has a normal distribution and that its mean value is 5 (we consider the data to have a measurement error equal to 10%), the null hypothesis of test 2 is that there is not an underlying trend in the β data and the null hypothesis of test 3 is that the β data are random and that they follow a normal distribution. The percentages refer to the level of confidence with which we can reject the null hypothesis.

Sample	Test 1	Test 2	Test 3
Abell (1- <i>mag</i> interval)	95 %	90 %	...
Coma (1- <i>mag</i> interval)	99 %	90 %	...
Hydra (1- <i>mag</i> interval)	...	90 %	...
Abell+Coma+Hydra (1- <i>mag</i> interval)	99 %	...	95 %
SDSS in each filter (1- <i>mag</i> interval)	99 %	95 %	...
SDSS sum of 4 filters (1- <i>mag</i> interval)	99 %	95 %	90 %
SDSS in each filter (0.5- <i>mag</i> interval)	99 %	95 %	...
SDSS sum of 4 filters (0.5- <i>mag</i> interval)	99 %	99 %	95 %
Abell+Coma+Hydra+SDSS sum of 4 filters (1- <i>mag</i> interval)	99 %	95 %	95 %

Table 7. KR coefficients for the SDSS simulation in r^* filter. Increasing magnitude intervals. MI is the absolute magnitude interval within which the galaxies are distributed, N is the number of galaxies in the magnitude interval, α_{Bis} is the zero point of KR, β_{Bis} is the slope of KR, σ_{KR} is the intrinsic dispersion of KR and R is the correlation coefficient of the fit (Pearson Statistics).

MI	N	α_{Bis}	β_{Bis}	σ_{KR}	R	MI	N	α_{Bis}	β_{Bis}	σ_{KR}	R
Simulation SDSS (r^* filter). Case 1.						Simulation SDSS (r^* filter). Case 2.					
$-20 \geq M > -21$	455	18.587 ± 0.015	4.971 ± 0.011	0.285	0.995	$-20 \geq M > -21$	140	18.533 ± 0.020	4.356 ± 0.032	0.234	0.968
$-20 \geq M > -22$	810	18.232 ± 0.022	4.865 ± 0.017	0.555	0.977	$-20 \geq M > -22$	280	18.313 ± 0.020	3.604 ± 0.023	0.330	0.953
$-20 \geq M > -23$	1065	18.029 ± 0.025	4.673 ± 0.022	0.785	0.945	$-20 \geq M > -23$	420	18.270 ± 0.019	3.213 ± 0.018	0.365	0.961
$-20 \geq M > -24$	1220	17.977 ± 0.025	4.442 ± 0.027	0.953	0.907	$-20 \geq M > -24$	560	18.277 ± 0.018	3.014 ± 0.013	0.381	0.971
$-20 \geq M > -25$	1275	17.995 ± 0.025	4.305 ± 0.031	1.030	0.885	$-20 \geq M > -25$	676	18.311 ± 0.017	2.872 ± 0.011	0.388	0.976
Simulation SDSS (r^* filter). Case 3.											
$-20 \geq M > -21$	245	18.602 ± 0.018	4.819 ± 0.025	0.275	0.984						
$-20 \geq M > -22$	439	18.360 ± 0.022	4.305 ± 0.027	0.478	0.943						
$-20 \geq M > -23$	579	18.338 ± 0.023	3.708 ± 0.028	0.585	0.906						
$-20 \geq M > -24$	664	18.412 ± 0.026	3.268 ± 0.029	0.627	0.889						
$-20 \geq M > -25$	669	18.474 ± 0.027	3.053 ± 0.028	0.640	0.887						

Table 8. KR coefficients for the SDSS simulation for r^* filter. Narrow $1 - mag$ intervals.

MI is the absolute magnitude interval within which the galaxies are distributed, N is the number of galaxies in the magnitude interval, α_{Bis} is the zero point of KR, β_{Bis} is the slope of KR, σ_{KR} is the intrinsic dispersion of KR and R is the correlation coefficient of the fit (Pearson Statistics).

MI	N	α_{Bis}	β_{Bis}	σ_{KR}	R	MI	N	α_{Bis}	β_{Bis}	σ_{KR}	R
Simulation SDSS (r^* filter). Case 1.						Simulation SDSS (r^* filter). Case 2.					
$-20 \geq M > -21$	455	18.587 ± 0.015	4.971 ± 0.011	0.285	0.995	$-20 \geq M > -21$	140	18.533 ± 0.020	4.356 ± 0.032	0.234	0.968
$-21 \geq M > -22$	355	17.614 ± 0.020	4.953 ± 0.016	0.284	0.992	$-21 \geq M > -22$	140	17.810 ± 0.024	4.356 ± 0.032	0.234	0.968
$-22 \geq M > -23$	255	16.677 ± 0.031	4.912 ± 0.025	0.280	0.985	$-22 \geq M > -23$	140	17.087 ± 0.033	4.356 ± 0.032	0.234	0.968
$-23 \geq M > -24$	155	15.878 ± 0.060	4.786 ± 0.048	0.270	0.963	$-23 \geq M > -24$	140	16.364 ± 0.045	4.356 ± 0.032	0.234	0.968
$-24 \geq M > -25$	55	15.727 ± 0.200	4.305 ± 0.147	0.212	0.885	$-24 \geq M > -25$	140	15.788 ± 0.069	4.356 ± 0.032	0.234	0.968
Simulation SDSS (r^* filter). Case 3.											
$-20 \geq M > -21$	245	18.602 ± 0.018	4.819 ± 0.025	0.275	0.984						
$-21 \geq M > -22$	194	17.709 ± 0.024	4.735 ± 0.032	0.269	0.976						
$-22 \geq M > -23$	140	16.984 ± 0.037	4.508 ± 0.043	0.253	0.960						
$-23 \geq M > -24$	85	16.697 ± 0.068	4.028 ± 0.065	0.218	0.925						
$-24 \geq M > -25$	35	17.391 ± 0.168	3.097 ± 0.119	0.140	0.891						

REFERENCES

- Akritas, M. G., & Bershad, M. A. 1996, *ApJ*, 470, 706
- Aguerri, J. L. A., Iglesias-Páramo, J., Vílchez, J. M., Muñoz-Tuñón, C., & Sánchez-Janssen, R. 2005. *ApJ*, 130, 475
- Bendat J. S., & Piersol A. G. 1966. *Measurement and Analysis of Random Data*. Ed. Wiley J. & Sons. New York.
- Bender, R., Burstein, D., & Faber S. M. 1996, *ApJ*, 463. L51
- Bender, R., Ziegler, B., & Bruzual, G. 1996, *ApJ*, 463. L51
- Bernardi, M., *et al.* 2003, *AJ*, 125, 1817
- Capaccioli, M., Caon, N., & D’Onofrio, M. 1992, *MNRAS*, 259, 323
- Djorgovsky, S., & Davies, M. 1987, *ApJ*, 313, 59
- D’Onofrio, M., Valentinuzzi, T., Secco, L., Caimmi, R., & Bindoni, D. 2006, *NewAR*, 50, 447
- Dressler, A., Lynden-Bell, D., Burstein, D., Davies, R. L., Faber, S. M., Terlevich, R., & Wegner, G. 1987, *ApJ*, 313, 42
- Faber, S. M., & Jackson, R. 1976, *ApJ*, 204, 668
- Fasano, G., Bettoni, D., Marmo, C., Pignatelli, E., Poggianti, B. M., Moles, M., & Kjærgaard, P. 2002, *ASPC*, 268, 361
- Fasano, G., Varela, J., Bettoni, D., *et al.* 2004, Private communication.
- Fukugita, M., Ichikawa, T., Gunn, J. E., Doi, M., Shimasaku, K., & Schneider D. P. 1996, *AJ*, 111, 4

- Graham, A. W., & Driver, S. P. 2005. PASP. 22. 118
- Graham, A., & Guzmán, R. 2003, AJ, 125, 2936
- Hamabe, M., & Kormendy, J. 1987, In: Structure and Dynamics of Elliptical Galaxies, IAU Symp., No 127, p.379, ed. de Zeeuw, T., Reidel, Dordrecht
- Hoessel, J. G., Oegerle, W. R., & Schneider, D. P. 1987, AJ, 94, 1111
- Isobe, T., Feigelson, E. D., Akritas, M. G., & Babu, G. J. 1990, ApJ, 364, 104
- Jorgensen, I., Franx, M., & Kærgaard, p. 1996, MNRAS, 280, 167
- Jorgensen, I., Franx, M., Hjorth, J., & van Dokkum, P. G. 1999, MNRAS, 308, 833
- Kelson, D.D., van Dokkum, P. G., Franx, M., Illingworth, G. D., & Fabricant, D. 1997, ApJ, 478, L13
- Kjærgaard, P., Jorgensen, I., & Moles, M. 1993, ApJ, 418, 617
- Kormendy, J., 1977, ApJ, 218, 333
- La Barbera, F., Busarello, G., & Capaccioli, M. 2000, A&A, 362, 851
- La Barbera, F., Busarello, G., Merluzzi, P., Massarotti, M., & Capaccioli M. 2003, ApJ, 595, 127
- Michard, R., 2000, A&A, 360, 85
- Milvang-Jensen, B. 1997, Master's Thesis. University of Copenhagen.
- Nigoche-Netro, A., Moles, M., Ruelas-Mayorga, A., Franco-Balderas, A., & Kjærgaard, P. 2007, A&A, 472, 773.

Reda, F. M., Forbes, D. A., Beasley, M., O’Sullivan, E. J., & Goudfrooij, P. 2004, MNRAS, 354, 851

Sandage, A., & Peremulter, J-M. 1991, ApJ, 370, 455

Sandage, A., & Lubin, L. M. 2001, ApJ, 121, 2271

Smith H., & Tinsley B. M. 1976, PASP, 88, 370

Treu T., Stiavelli M., Bertin G., Casertano S., & Moller P. 2001, MNRAS, 326, 237

Varela, J. 2004, PhD Thesis. Universidad Complutense de Madrid.

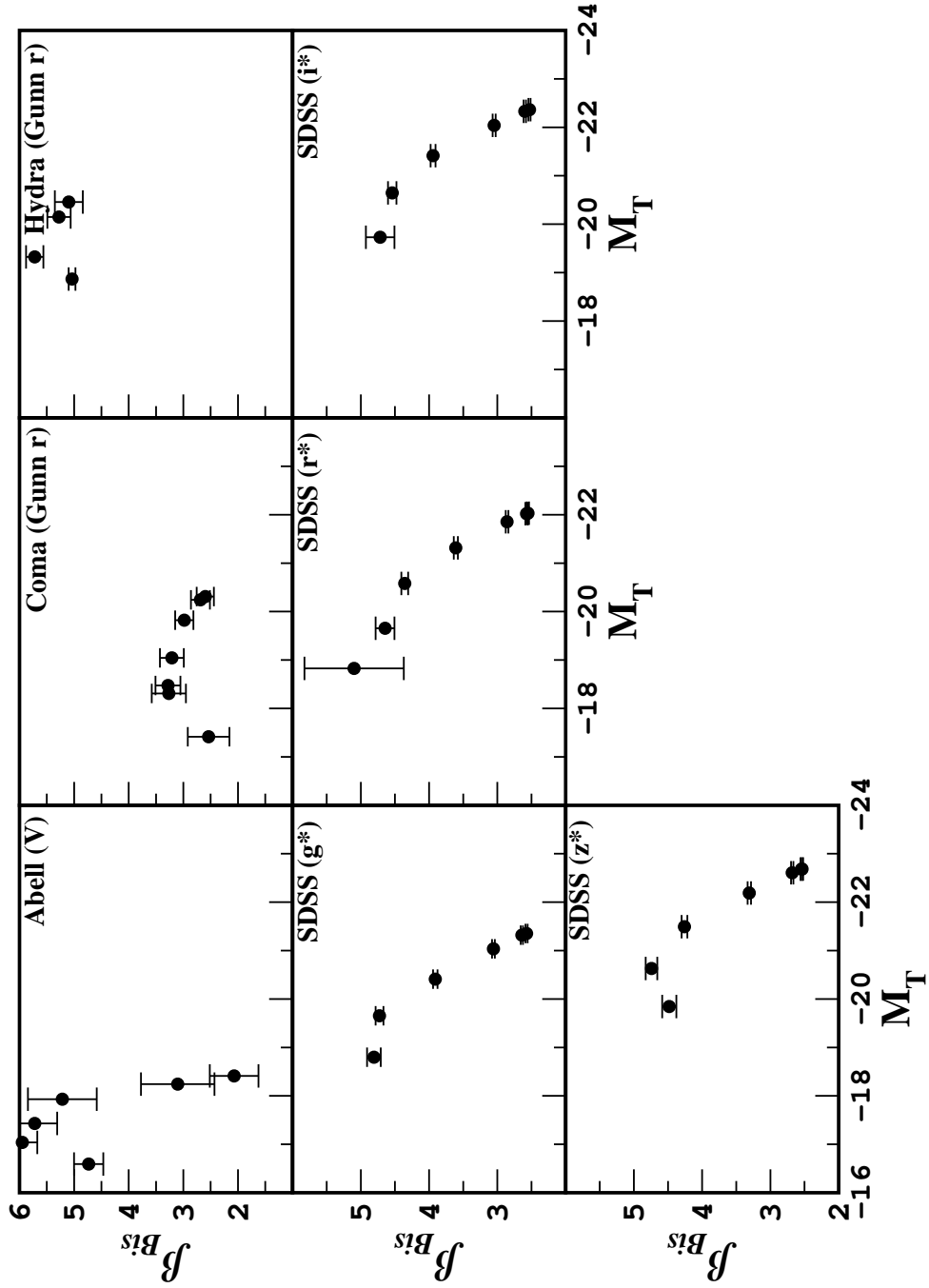


Fig. 1.— Graph of the variation of the KR slope (β) for the different samples of galaxies in increasing magnitude intervals. This graphs shows the β coefficient obtained using the $BCES_{Bis}$ method. Each point corresponds to the mean value of the magnitude of the galaxies contained in each magnitude interval (see table 2). Filters g^* , r^* , i^* and z^* correspond approximately to Johnson-Morgan-Cousins filters B, V, R_c and I_c respectively (Fukugita et al. 1996).

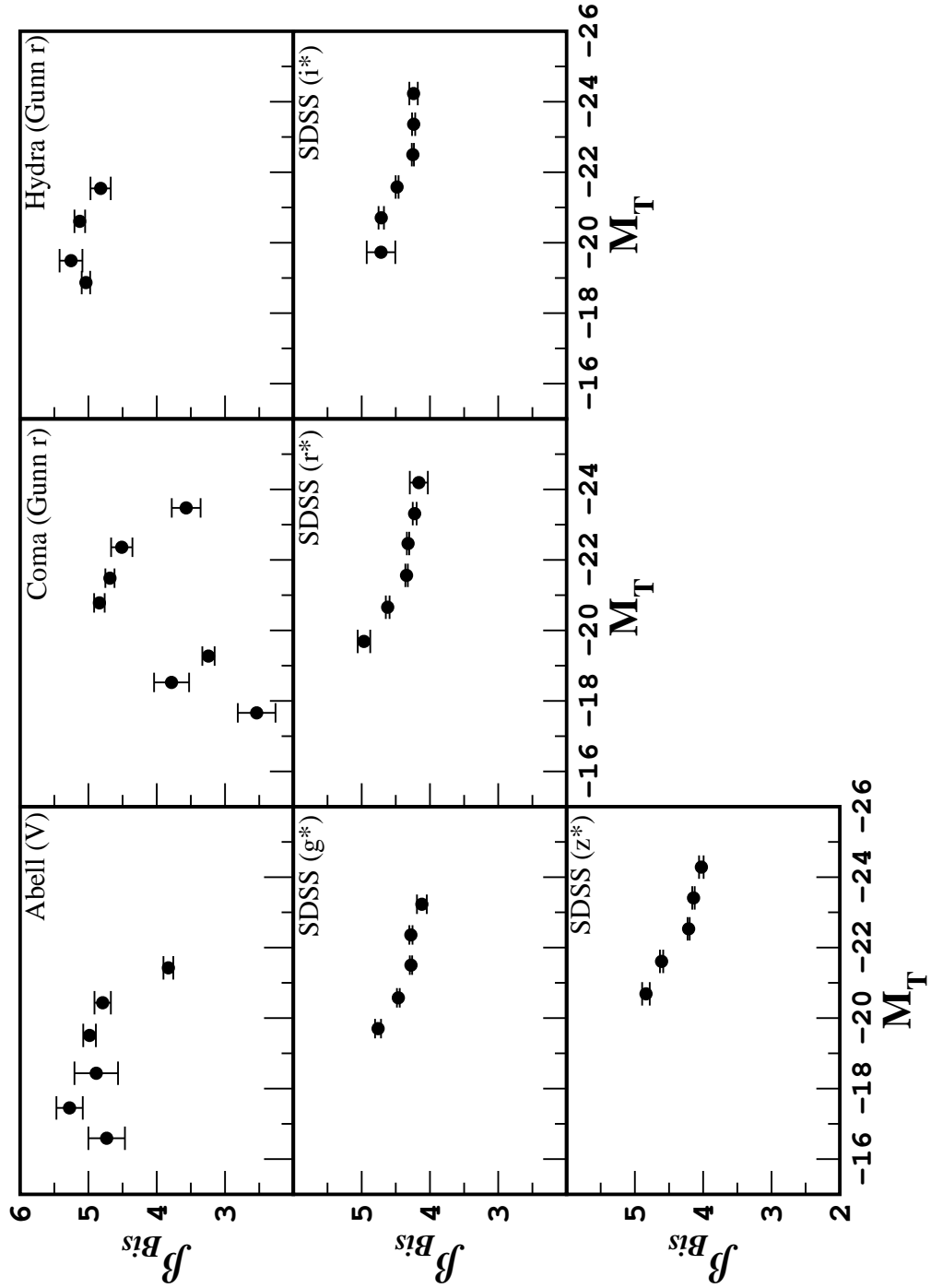


Fig. 2.— Variation of the KR slope (β) for the different samples of galaxies. The graphs show the β coefficient values obtained with the $BCES_{Bis}$ method. Each point represent a 1 – mag interval (mean value of the magnitude of the galaxies contained in each magnitude interval analyzed, see table 3).

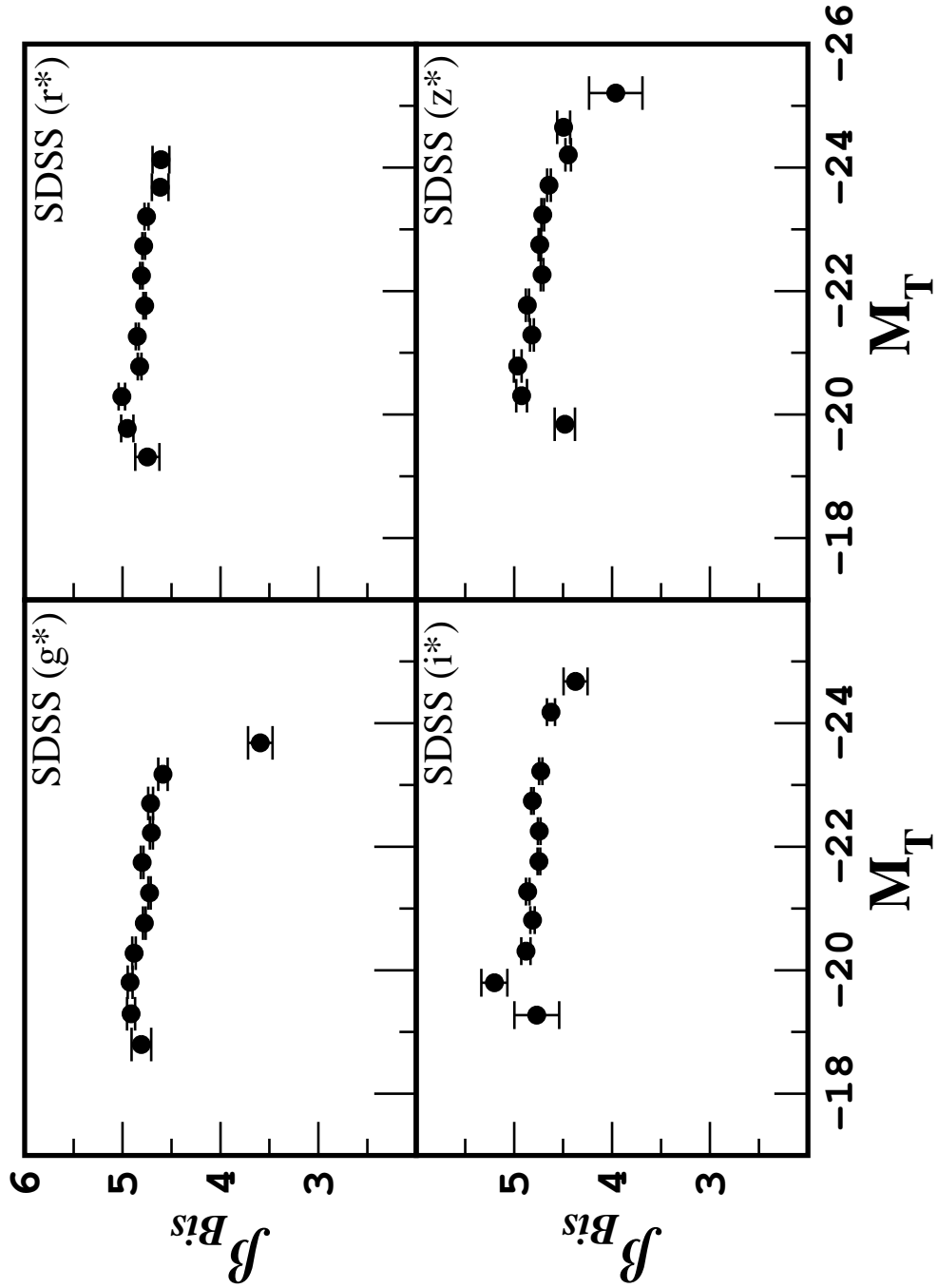


Fig. 3.— Variation of the KR slope (β) for the SDSS galaxies (g^* , r^* , i^* and z^* filters). Graphs show the data for the β coefficient obtained by the $BCES_{Bis}$ method. Each point represents a 0.5 – mag interval (mean value of the magnitude of the galaxies contained in each magnitude interval analyzed, see table 4).

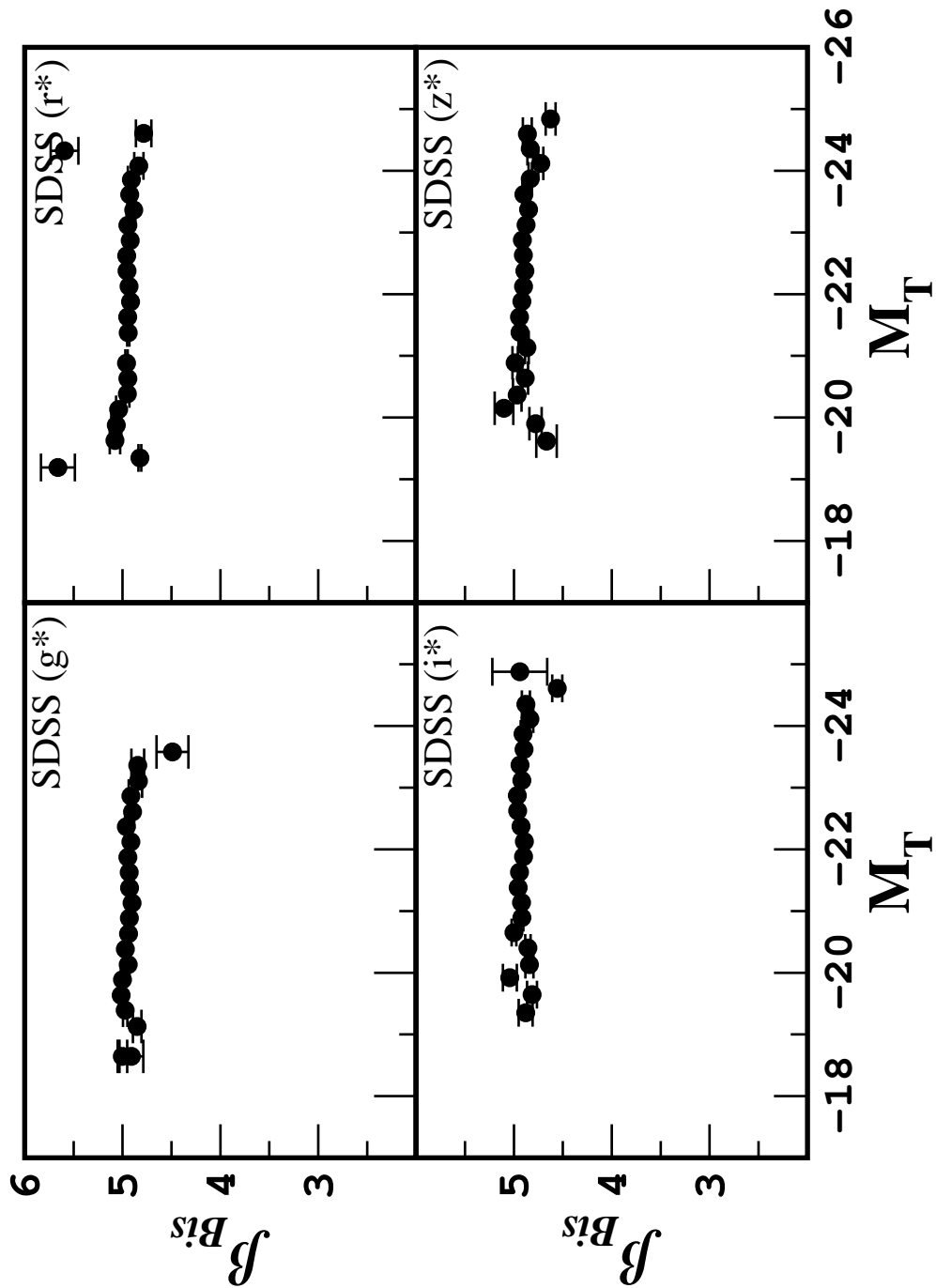


Fig. 4.— Variation of the KR slope (β) for the SDSS galaxies (g^* , r^* , i^* and z^* filters). Graphs show the data for the β coefficient obtained by the $BCES_{Bis}$ method. Each point represents a 0.25 – mag interval (mean value of the magnitude of the galaxies contained in each magnitude range analyzed, see table 5).

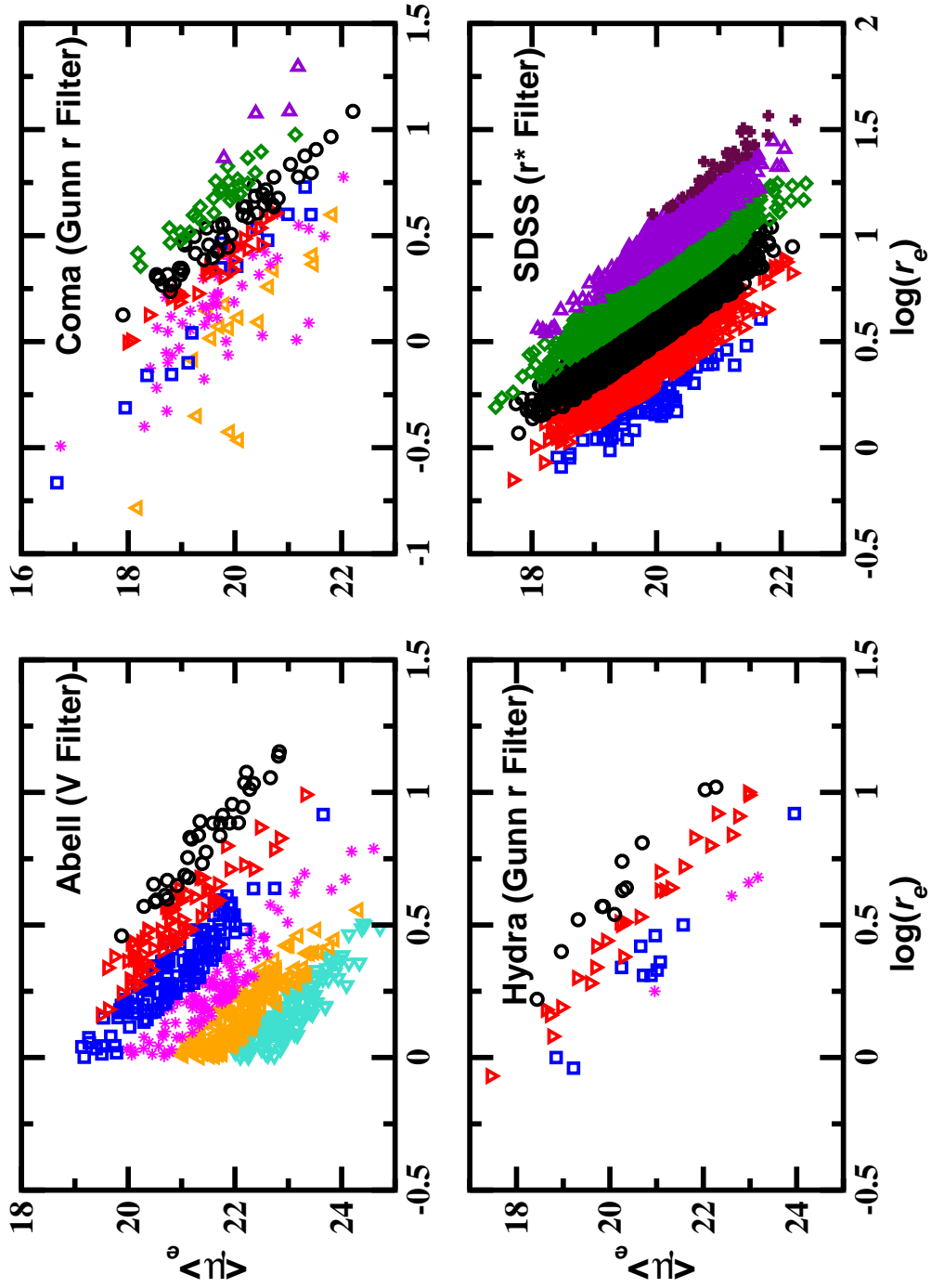


Fig. 5.— Distribution of the Abell, Coma, Hydra and SDSS (r^* filter) galaxies on the $\log(r_e) - \langle \mu \rangle_e$ plane. Each symbol represents a 1 $- mag$ interval. The circles represents the $[-21, -22]$ mag interval.

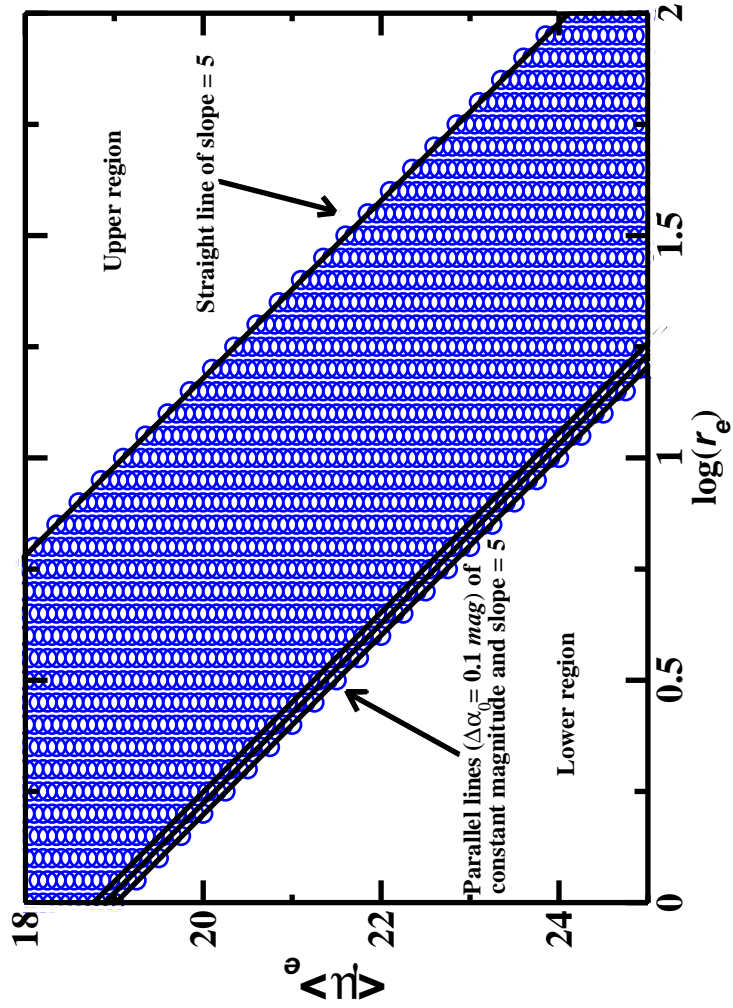


Fig. 6.— Distribution of simulated galaxies on the $\log(r_e) - \langle \mu \rangle_e$ plane. The data distribution consists in parallel lines of slope 5 which shift to brighter magnitude.

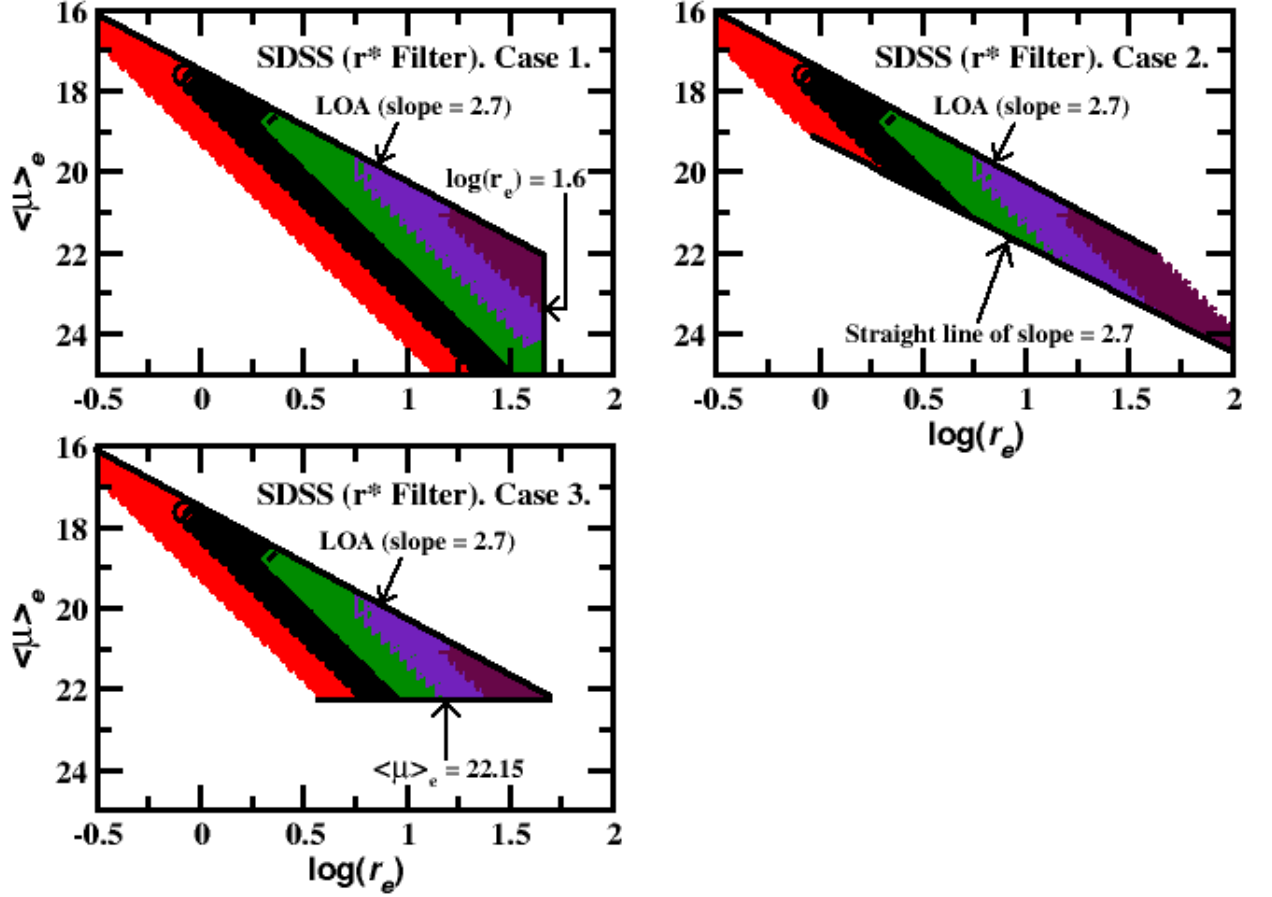


Fig. 7.— Distribution of simulated SDSS galaxies (r^* filter) on the $\log(r_e) - \langle \mu \rangle_e$ plane. Each symbol represents a 1-mag interval. The circles represents the $(-21, -22]$ mag interval. Case 1: upper region of the diagram, limited by a straight line of slope 2.7 (LOA) (D’Onofrio et al. 2006) and radius limit ($\log(r_e) \leq 1.6$) for all the magnitude intervals. Case 2: upper and lower regions of the diagram limited by a straight line of slope 2.7. Case 3: upper region of the diagram limited by a straight line of slope 2.7 and brightness limit ($\langle \mu \rangle_e \leq 22.15$ mag/arcsec²) for all the magnitude intervals.

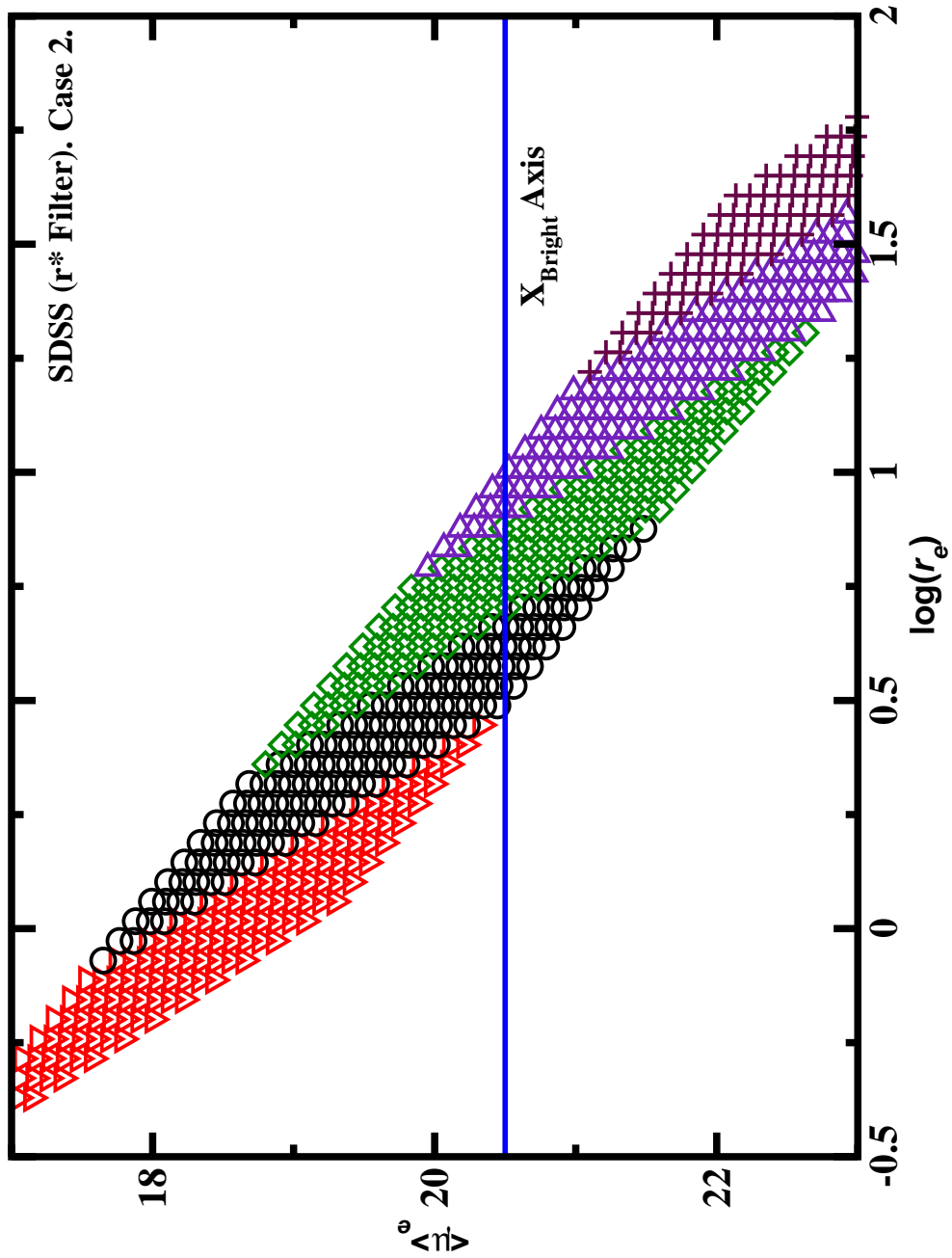


Fig. 8.— Distribution of simulated SDSS galaxies (r^* filter) on the $\log(r_e) - \langle \mu \rangle_e$ plane (Case 2). Each symbol represents a 1-mag interval. The solid line (X_{Bright} -axis) is a line of slope=0 that contains the barycenter of the distribution of the galaxies. The galaxy distribution is symmetrical under a reflection with respect to the X_{Bright} -axis and a 180° rotation with respect to a perpendicular line to the X_{bright} -axis that contains the barycenter of the galaxy distribution.

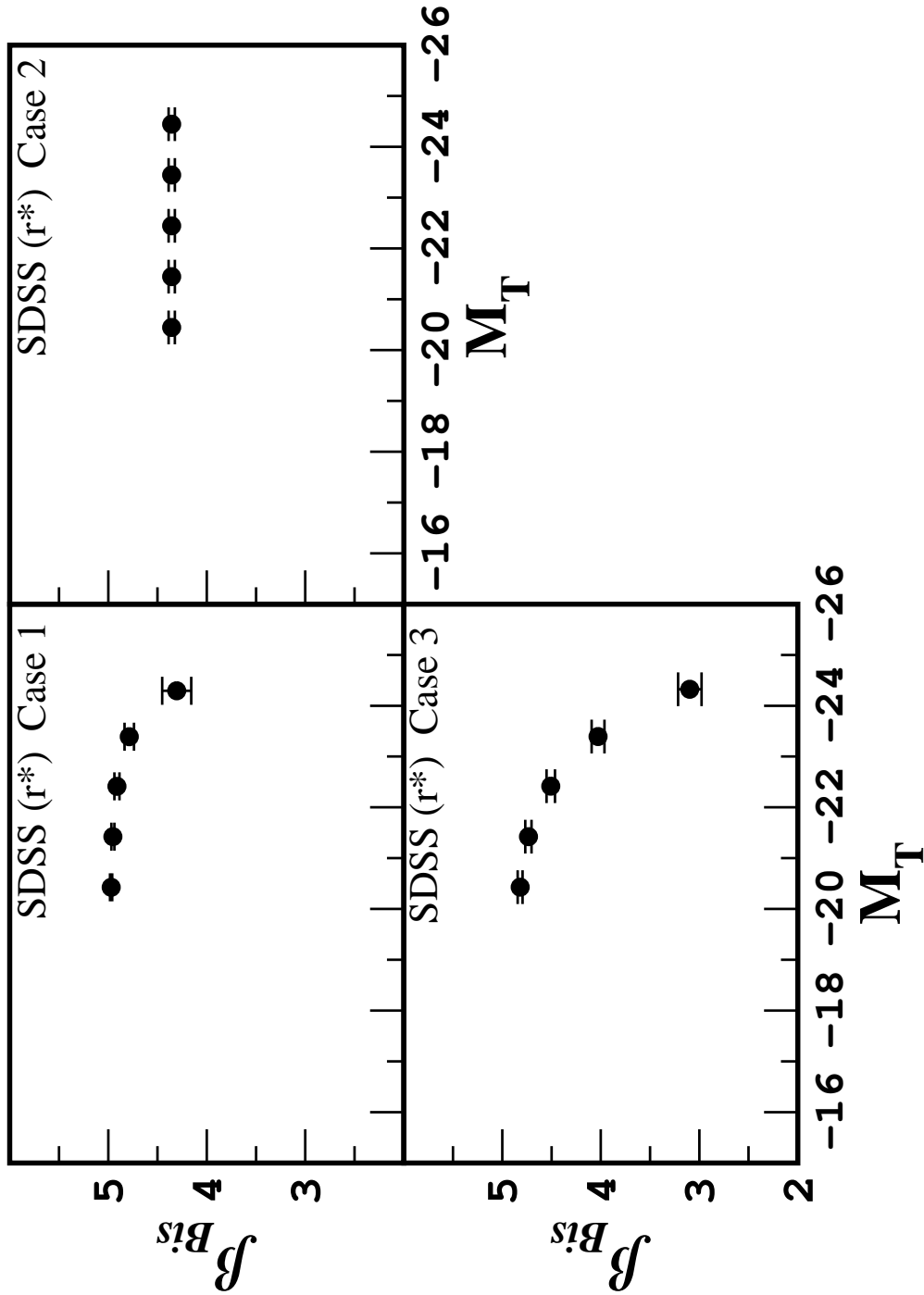


Fig. 9.— Variation of the KR slope (β) for one of the SDSS simulations (r* filter). Graphs show the data for the β coefficient obtained by the $BCES_{Bis}$ method. Each point represents a 1-mag interval (mean value of the magnitude of the galaxies contained in each magnitude range analyzed, see table 8).